Bio-inspired self-healing polymer foams with bilayered capsule systems

Shunze Cao[1], Wen Zhu[2], Tao Liu[1,3,*]

[1]Centre for Structural Engineering and Informatics, Faculty of Engineering, University of Nottingham, University Park, Nottingham, NG7 2RD, United Kingdom

[2]Advanced Materials Research Group, Faculty of Engineering, University of Nottingham, University Park, Nottingham, NG7 2RD, United Kingdom

[3]Composites Research Group, Faculty of Engineering, University of Nottingham, University Park, Nottingham, NG7 2RD, United Kingdom

[*]Corresponding author - Email: Tao.Liu@nottingham.ac.uk, Tel: + 44 (0)115 7484059

Submitted Date: October 16, 2019

Abstract

Bio-inspired, self-healing polymer foams containing novel calcium-alginate capsule system was developed for load-bearing application. The capsules were created by a multi-stage encapsulating process that can encapsulate two mutually reactive healing agents within single capsules. The capsules had a bilayered structure with the epoxy resin encapsulated within the inner layer and the hardener within the outer layer. To evaluate the mechanical self-healing performance, the following tests were conducted, i.e. (1) cyclic quasi-static compression tests for foams; (2) quasi-static three-point bending tests for foam core sandwich beams; and (3) high-speed soft impact tests for foam core sandwich beams. Cyclic quasi-static compression tests demonstrated (1) bilayered capsule systems had better multiple self-healing effect compared to the dual capsules system without external interventions; and (2) bilayered capsules could enhance the stiffness and strength of foams. For foam core sandwich beams, the bilayered capsules did not have a noticeable effect on the effective stiffness of the beams; however, it could provide a noticeable self–healing effect when the damage occurred. The images obtained from scanning electron microscope (SEM) and X-ray microcomputed tomography (μCT) suggested that the micro-cracks induced by the static and impact loading were either fully or partially healed by the released healing agents without external interventions.

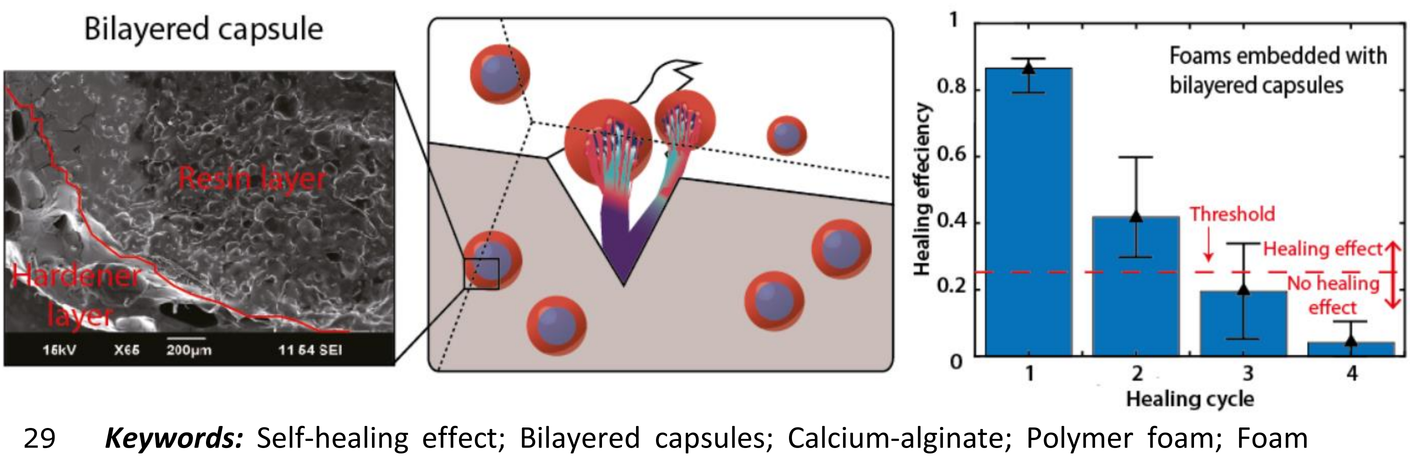

Keywords: Self-healing effect; Bilayered capsules; Calcium-alginate; Polymer foam; Foam core sandwich beams

1. Introduction

Composite wind turbine blades, consisting of fibre reinforced composites and foam core sandwich structures, may subject to a wide range of physical events during the life expectancy. These events may include variable amplitude cyclic loadings, bird strike, lightning strike as well as daily and seasonal temperature and humidity variations [1-4], which may incur various damage in the composite structures. Dramatic growth in off-shore wind farms has created opportunities for the application of large scale wind turbine systems in order to achieve high power generation efficiency. The system of power level 12 MW and rotor diameters on the order of 220 m Haliade-X has recently been under development [5]. However, large scale wind turbine systems may subject to difficulty in maintenance and damage repair, especially, for the wind farms far away from the shore. Here, we report a novel, bio-inspired [6] self-healing polymer foams that can be combined with fibre reinforced polymer composites to create self–healing foam core sandwich structures for composite wind turbine blade systems. The self-healing function embedded in the material systems will automatically be activated to fully or partially restore the functionality of the composite materials when damage occurs.

For polymer composites, self-healing can be achieved through intrinsic and extrinsic self-healing mechanisms [7-9]. Intrinsic self-healing is activated by the parent polymers under external stimuli, including various thermo-mechanical/chemical stimuli. Hayes et al. (2007) developed intrinsic solid state self-healing systems that could achieve multiple healing effects. The healing agent was pre-mixed in the epoxy resin at 80 ^{0}C , and the damaged samples could be healed at the temperature over 100 ^{0}C [10, 11]. Li and John (2008) and John and Li (2010) developed self-healing synthetic foam core sandwich structures. The synthetic foam core had the functionality of shape memory, and damage recovery could be achieved through a multistep heating process [12, 13].

Extrinsic self-healing can be achieved through releasing the prefilled healing agents within either vascular [14, 15] or capsular [16, 17] containers when damage occurs. Capsular self-healing systems are suitable for industrial-scale production with the advantages of easy fabrication, low cost, and versatility [18]. The two-part healing agents (resin and hardener) can be encapsulated through three approaches, i.e. dual-capsule system [19], capsules-catalysts system [20], and mono-capsules system [21, 22]. In the dual-capsule system, the capsules containing resin and the capsules containing hardener coexist inside the material systems, as shown in Fig. 1(a). The healing effect can be achieved when the released resin and hardener are mixed at the locations of damage. Yuan et al. (2008) encapsulated diglycidyl tetrahydro-*o*-phthalate (DTHP) (resin) and mercaptan/tertiary amine (hardener) using the dual-capsule system. The dual capsules were then embedded into the EPON polymer matrix. Tapered double cantilever beam tests were conducted to evaluate the healing effects, which indicated that the healing efficiency reached 100% when the capsules concentration (wt.%) was more than 5% [23]. Hia et al. (2018) fabricated a dual capsules system, which contained diglycidyl ether of bisphenol A (resin) and mercaptan/tertiary amine (hardener). The specimens were tested by an impact pendulum, which revealed that the maximum healing efficiency reached over 55% when the capsules concentration was 20% [24]. Except for the mercaptan/tertiary amine, Li et al. (2013) selected polyetheramine (D-230) as the hardener. The healing efficiency reached 84.5% with 15 wt.% of capsules. However, if the capsules were not uniformly distributed, the released resin and hardener agents could not be well mixed to achieve good healing effects [25].

In the capsules-catalysts based self-healing system, catalysts are pre-dispersed within the matrix. The healing effect is initiated when the healing agent is released from the cracked capsules and interacts with the catalysts. White et al. (2001) tested the EPON polymer matrix embedded with dicyclopentadiene (DCPC) capsules and bis (tricyclohexylphosphine) benzylidene ruthenium (IV) dichloride catalyst under mode I fracture tests. The healing efficiency was 45% at room temperature when capsules concentration was 5%. The healing efficiency increased to 80% in the 80 ^{o}C environment [26]. Later on, several capsules-catalysts based self-healing systems were developed including the DCPD healing agents with the WCl_6 catalysts [27], the ENB blend healing agents with the Grubbs' catalysts [28] and the ethyl phenylacetate (EPA) healing agents with the solid-state catalysts $(Sc(OTf)_3)$ [29]. The healing efficiency of the above capsules-catalysts systems ranged from 40% to 110% depending on the capsule concentration and temperature. The additional cost and toxicity of the catalysts limited their applications [30].

The mono-capsules system only contains capsules with single-part healing agent. Healing effects are triggered when the resin releases from capsules and flows through cracks. Several ideas for developing mono-capsules systems were proposed by different researchers. Caruso et al. (2008) developed two epoxy solvent-based self-healing systems, namely, chlorobenzene and ethyl phenylacetate solvents. When solvents were released from capsules and encountered the residual amine existing in the matrix, the healing effect was triggered [31]. The healing efficiency could reach 100% with 15wt.% capsules in the 35 ^{o}C environment. Yuan et al. (2013) fabricated a mono-capsules system, which contained diaminodiphenylsulfone (DDS) catalysts agents. The capsules were embedded into the cyanate ester (CE) polymer matrix. Fracture toughness was measured using single-edge notched beams under Mode I conditions [32]. The healing effect was triggered when the released DDS encountered the melted CE resin. The healing efficiency was 85% at 220 ^{o}C environment when capsules concentration was 5%. Unlike the dual capsules based systems, the mono-capsules based self-healing system does not require the uniform dispersion of two types of capsules. However, the requirements of external interventions and the toxicity of solvents limited their applications.

In this research, we report a novel, multi-stage encapsulating process that can encapsulate epoxy resin and hardener within single calcium-alginate capsules. The capsules have a bilayered structure with epoxy resin stored in the inner layer and hardener stored in the outer layer, as schematically shown in Fig. 1 (b). Upon the damage events occurred inside of the materials, both healing epoxy resin and hardener can be released from the capsules to repair the voids and cracks within the damaged areas without imposing heat and pressure. To evaluate of the self-healing performance, polymer foams and sandwich beams, both embedded with bilayered capsules, were fabricated and tested under static and impact loadings.

2. Materials and manufacturing

2.1. Materials

The polymer foams

The polymer foams were created by mixing PB250 epoxy resin[1] and DM03 hardener[1]. The PB250 epoxy resin consisted of bisphenol A diglycidyl ether (DGEBA) and epoxide derivatives, which had a density of 1.10 $\mathrm{g/cm^3}$ and a viscosity of 10000 – 14000 mPa•s at 25 $^{0}\mathrm{C}$. The DM03 hardener consisted of triethylentetramine (TETA), phenol, formaldehyde/phenol/TETA polymer, diethylenetriamine (DETA), and alkyl ether polyamine, which had a density of 1.00 $\mathrm{g/cm^3}$ and a viscosity of 170 – 250 $\mathrm{mPa{\bullet}s}$ at 25 $^0\mathrm{C}$. The mix ratio was 100 weight of resin with 30 weight of hardener. The mixed emulsion was cured after 6 hours at 40 $^0\mathrm{C}$. The compressive strength and elastic modulus of the cured foams after free expansion were 6 MPa and 240 MPa, respectively. A cubic aluminium mould with the inner edge length $l_a = 50\ \mathrm{mm}$ was used to fabricate the specimen in the foaming process. The cured polymer foams had the closed-cell microstructure with the density of $\rho_e = 0.33\mathrm{g/cm^3}$, the volume fraction of void of $n_v = V_v/V_T = 0.65$, where V_v is the volume of void and V_T the total volume, as shown in Fig. 1 (c). The low water absorption ensured that the majority of the released healing agents could flow through the micro-cracks and the fractured cells. The internal microstructure of the cured foam was examined via scanning electron microscopic (SEM) images, see Fig. 1(c) for example, which showed that the average diameter of the pores within the foam samples was $d_c = 0.16\mathrm{mm}$. The bilayered calcium-alginate capsules were added to the mixture at the beginning of the foaming process, which can be uniformly distributed within the foams.

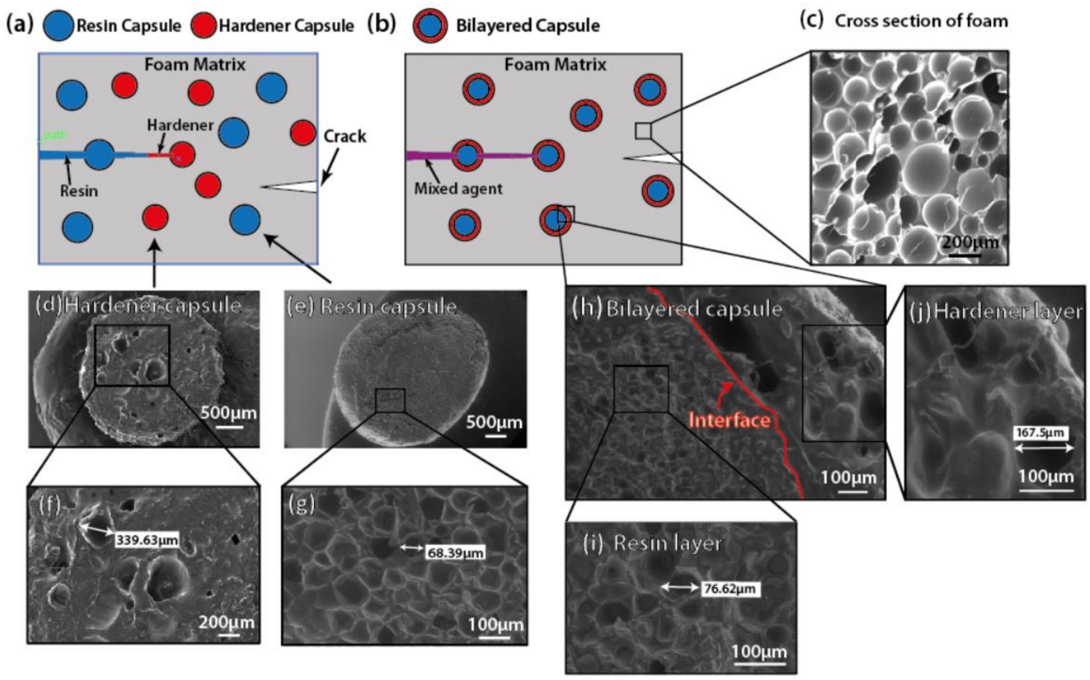

Figure 1. The schematics of (a) the dual-capsule self-healing system, and (b) the bilayered capsule based self-healing system. (c) The SEM image of the microstructure of the polymer foam. The SEM images of a hardener capsule showing a multicore-like internal microstructure ((d) and (f)) ; the SEM images of a resin capsule showing an irregular honeycomb-like internal microstructure ((e) and (g)); and the SEM images of a bilayered capsule showing a multicore-like internal microstructure at the

hardener layer and an irregular honeycomb-like internal microstructure at the resin layer ((h), (i) and (j)).

The two-part healing agents

The epoxy rapid repair resin[2] and formulated amine hardener[2] were used as the healing agents and encapsulated within the sodium-alginate capsules. The rapid repair epoxy resin consisted of bisphenol A, 1,4 – butanediol diglycidyl ether, propylene carbonate, and 1,3 – propanediol, which had a density of 1.16 – 1.21 g/cm^3 and a viscosity of 900 – 1300 $mPa{\bullet}s$ at 25 ^0C. The formulated amine hardener consisted of aminoethylpiperazine, nonylphenol, triethanolamine, and 2,4,6 – tris, which had a density of 0.94 – 0.99 g/cm^3 and a viscosity of 120 – 160 $mPa{\bullet}s$ at 25 ^0C. The mix ratio by weight was 100:33 (rapid repair resin to formulated amine hardener), which gave a viscosity of 800 – 1200 $mPa{\bullet}s$ at 25 ^0C for the mixed agents. The curing time was 15 minutes at room temperature. This epoxy system had several advantages to achieve potential high self-healing efficiency. Firstly, the mixed agents had low viscosity, which enabled the fast-flowing of healing agents through the cracked media. Secondly, the mixed agent could be cured quickly, and the cured material had good recovery of mechanical properties. The tensile strength, flexural strength and flexural modulus of the polymerized healing agents were 40 – 50 MPa, 95 – 105 MPa and 2200 – 2700 MPa, respectively.

2.2. The two-stage encapsulation process

The microstructures of capsules were formed through the chemical reaction when sodium alginate[3] ($C_6H_7O_6Na$) encountered calcium chloride[3] ($CaCl_2{\bullet}H_2O$). A two-stage encapsulation process was employed to create the bilayered capsules, as shown in Fig. 2. For the first stage, the inner resin layer was fabricated, as shown in Fig. 2 (a). 40*g* epoxy rapid repair resin was mixed with 50*g* deionized water by the Digital Overhead Stirrer OS-40 for 15 min. Then, 1.5g sodium alginate powder was added into the well-mixed resin solution in three portions at the interval of 15 minutes. The well-mixed resin-alginate emulsion was dropped into the 0.02 wt% calcium chloride solution from a 1000 ml dropping funnel with a 2 mm socket size. The calcium ions replaced the sodium ions of sodium alginate in the droplets and cross-linked the alginate polymer to form resin layer capsules [33]. The resin layer capsules

1 Matrix Composites Ltd. UK
2 Easy Composites Ltd. UK
3 Sigma-Aldrich
4 RS Components

were then sieved out from the calcium solution and washed by the deionized water. To evaporate water from capsules, the capsules were placed into an oven with 40 ^{0}C for 3 hours [16, 24]. The diameter of dried resin layer capsules ranged from 3mm to 3.5mm. For the second stage, the outer hardener layer was fabricated. The dried single layer resin capsules were mixed with alginate-hardener emulsion. A laboratory stirrer was used to mix the emulsion and capsules for 15 minutes to make sure the good covering of emulsion on the surface of the resin capsules. The emulsion covered capsules were sieved out and dropped into the 0.02 wt% calcium solution to form the outer alginate-calcium microstructure containing the hardener agent. The fabrication process of the second stage is shown in Fig. 2 (b). The bilayered capsules were sieved out of calcium solution and dried in an oven with 40 ^{0}C for 3 hours to evaporate water. The diameters of the dried bilayered capsules ranged from 3.5mm to 4mm. For the comparison purpose, single layer capsules containing either resin or hardener agent were fabricated to create polymer foams with dual-capsule healing system based on the first stage. The internal structures of a bilayered capsule and a single layer capsule are shown in Fig. 1(d) to (g).

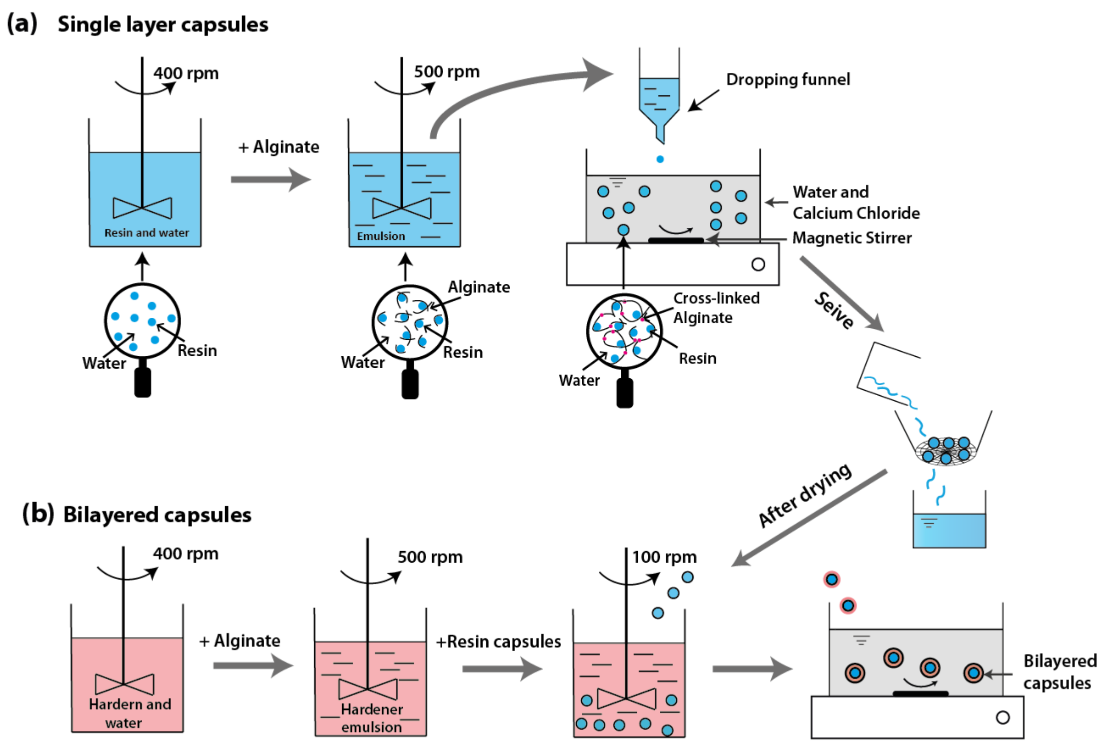

Figure 2. The schematics of the two-stage encapsulation process: (a) inner layer, and (b) outer layer.

2.3. Characterisation of capsules

To characterise the internal structures of capsules, a resin capsule, a hardener capsule, and a bilayered capsule were cut by a stainless steel blade and dried within a vacuum oven to evaporate healing agents before processing by scanning electron microscope (SEM). The SEM images of the hardener capsule, resin capsule, and bilayered capsule are shown in Fig. 1(d), (e) and (h), respectively. The hardener capsule has a multicore-like internal microstructure that provides space to store healing agent, as shown in Fig. 1 (f), which is similar to that of outer layer in the bilayered capsule, as shown in Fig. 1 (j). The epoxy resin capsule has an irregular honeycomb-like internal microstructure to store resin agent, as shown in Fig. 1 (g), which is similar to that of inner layer in the bilayered capsule, as shown in Fig. 1 (i).

2.4. Thermal characterisation of capsules

The thermogravimetric analysis (TGA) was applied to evaluate the thermal stability of healing agents and capsules. The NETZSCH, TG 499 F3 Jupiter Machine with the nitrogen flowing atmosphere and 10 $^{0}\mathrm{C/min}$ heating rate was used. Three capsules or 5g healing agent were placed in an aluminium crucible in each analysis. Fig. 3 (a) shows the TGA results of the resin agents (solid curve) and resin capsules (dashed curve). Both resin agents and capsules had a slight mass loss up to 250 $^{0}\mathrm{C}$ owing to the absorption of moisture by specimens. The dramatic mass losses occurred between 250 $^{0}\mathrm{C}$ and 450 $^{0}\mathrm{C}$. Fig. 3 (b) shows the TGA results of the hardener agents and hardener capsules, respectively. A dramatic mass losses were observed between 200 $^{0}\mathrm{C}$ and 220 $^{0}\mathrm{C}$. As the healing agents were nearly evaporated with the rise of temperature, the residual mass of capsules could be mainly attributed to the decomposed materials from the calcium-alginate microstructures. As shown in Fig. 3 (c), the mass of capsules without healing agents decreases gradually with the increase of temperature because of the removal of the crystalline water from calcium chloride ($\mathrm{CaCl_2{\bullet}H_2O}$) between 150 $^{0}\mathrm{C}$ and 220 $^{0}\mathrm{C}$ and the decomposition of sodium alginate ($\mathrm{C_6H_7O_6Na}$) to $\mathrm{Na_2{\bullet}CO_3}$ and the carbonized material between 550 $^{0}\mathrm{C}$ and 750 $^{0}\mathrm{C}$.

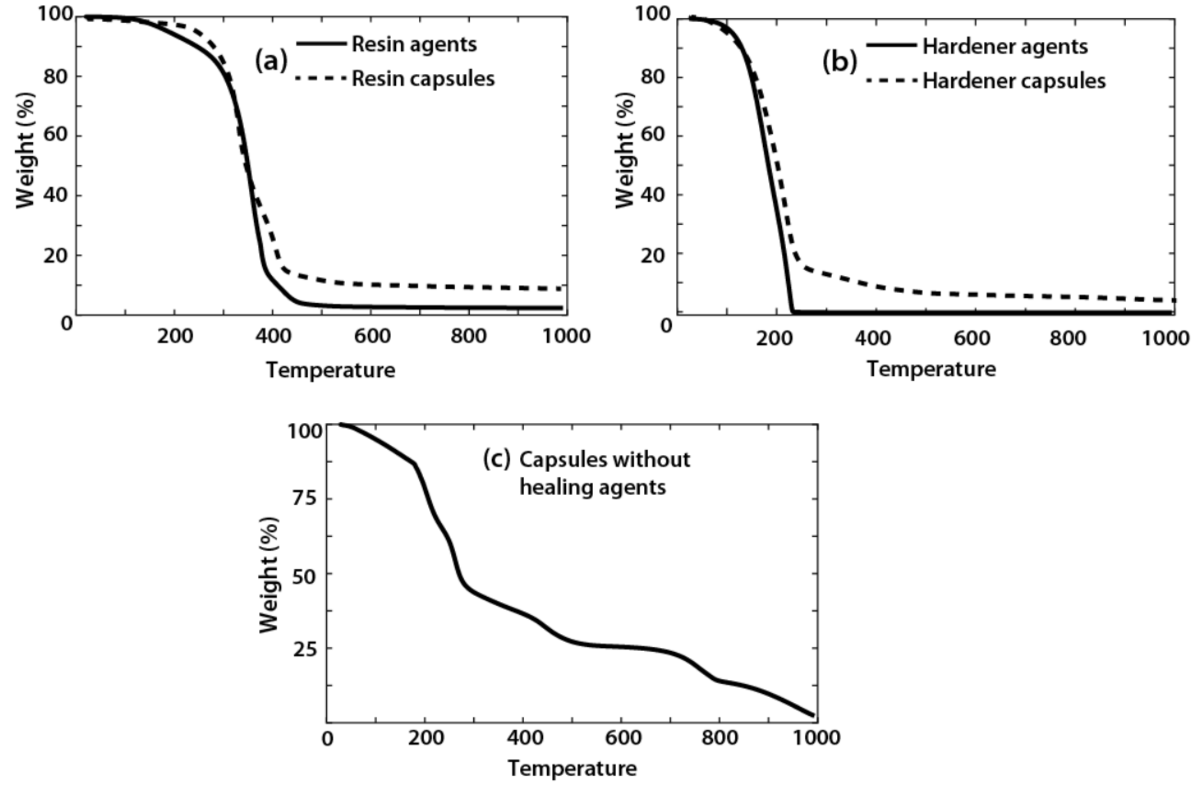

Figure 3. The TGA analysis of the (a) epoxy resin agents and resin capsules, (b) hardener agents and hardener capsules, and (c) capsules without healing agents.

2.5. Fabrication of the polymer foams

Polymer foams without fibre reinforcements

A cubic aluminium mould with a 50 mm inner edge length was used to fabricate polymer foams. Before fabrication, the Macwax non-silicone aerosol release agents[1] were spread on the internal surfaces of the mould for the ease of de-moulding. The foaming process was triggered by the chemical reaction between the PB250 resin and DM03 hardener. To fabricate neat foam samples, the PB250 resin and DM03 hardener were mixed at the weight ratio of 10:3 for 5 minutes using Digital Overhead Stirrer at the speed of 500 r/min. The mixed emulsion was then transferred into the aluminium mould. After the emulsion expanded to the top of the mould, the mould was tightly sealed and placed into an oven to cure at 40 $^0\mathrm{C}$ for 24 hours. The density of the neat foam samples was 350-400 kg/m^3. To fabricate foam samples containing capsules, the dried capsules were mixed with the emulsion before being transferred into the aluminium mould. The dimension of foam samples after cure was 50mm X 50mm X 50mm.

Polymer foams with fibre reinforcements

The CEM-FIL® short glass fibres[4] were employed to reinforce foam cores in sandwich beams to provide flow channels and facilitate the healing mechanisms. The volume fraction of the embedded short fibres $n_s = \Omega_{sh}/\Omega$ was 3.73%, where Ω_{sh} is the volume of embedded short fibres. During the fabrication, short fibres were mixed with the emulsion before transferring into the mould. Three dimensions of glass fibre reinforced polymer foams were fabricated, which were 240mm X 40mm X 10mm for three-point bending tests, 50mm X 50mm X 50mm for quasi-static compressive tests, and 140mm X 40mm X 10mm for shear tests.

2.6. Fabrication of sandwich beams

A sandwich beam was manufactured by bonding two identical glass fibre reinforced epoxy laminates on the top and bottom sides of the foam core via the Loctite EA 9461 two-part adhesive[4]. The adhesive was cured at 40 $^0\mathrm{C}$ under 2KPa dead load for 24 hours to ensure the stable bonding. In this study, sandwich beam samples embedded with 15% VF bilayered capsules, 15% VF resin capsules, and without capsules were fabricated.

3. Experiments

3.1. Cyclic quasi-static uniaxial compression test

Cyclic quasi-static uniaxial compressive tests of polymer foams

As the foams are mainly under compressions in the engineering applications, cyclic quasi-static compression tests were conducted to induce damage within the foam matrix and to examine the self-healing effects. Cubic specimens with an edge length of $50 \ \mathrm{mm}$ embedded with bilayered capsules, dual capsules, resin capsules in 10% volume fraction (VF), and neat foams (without capsules) were fabricated for testing. The neat foams and foams embedded with resin capsules were designed as the control groups which had no healing effects. The self-healing efficiencies of foams embedded with dual capsules and foams embedded with bilayered capsules were compared. The schematic of the experimental setup is shown in Fig. 4 (a). The tests were carried out by an Instron Universal Testing Machine at room temperature following the procedure ASTM 1621-04a with three repetitions for each type of specimen. The displacement-controlled crosshead speed of the test machine was 5 $\mathrm{mm/min}$. The measured compressive force P_F and the vertical displacement Δl of the crosshead were recorded by a 50KN load cell and Linear Variable Differential Transformer (LVDT), respectively. Let l_{0r} and l represent the original height and final height of a foam sample, and *A* the original area of the cross-section of the sample, *A*= l_{0r}^2 . The compressive strain and stress of the foams were calculated as $\varepsilon = |l - l_{0r}| / |l_{0r}|$ and $\sigma = P_F / A$, respectively. In the cyclic compression test, a compression cycle contained a loading phase and an unloading phase, see Fig. 4 (f). Let ε_n represents the compressive strain after a loading phase in the compression cycle n , $n = \{1,\ 2,\ 3,\ 4\}$. The applied compressive strain was controlled based on the relation $\varepsilon_n = \varepsilon_{n-1}^* + 0.075$ to achieve adequate damage before densification, where ε_{n-1}^* is the residual strain measured after the unloading phase in the $(n-1)$ compression cycle, and $\varepsilon_0^* = 0$. The interval time between two compression cycles was 24 hours to achieve stable results.

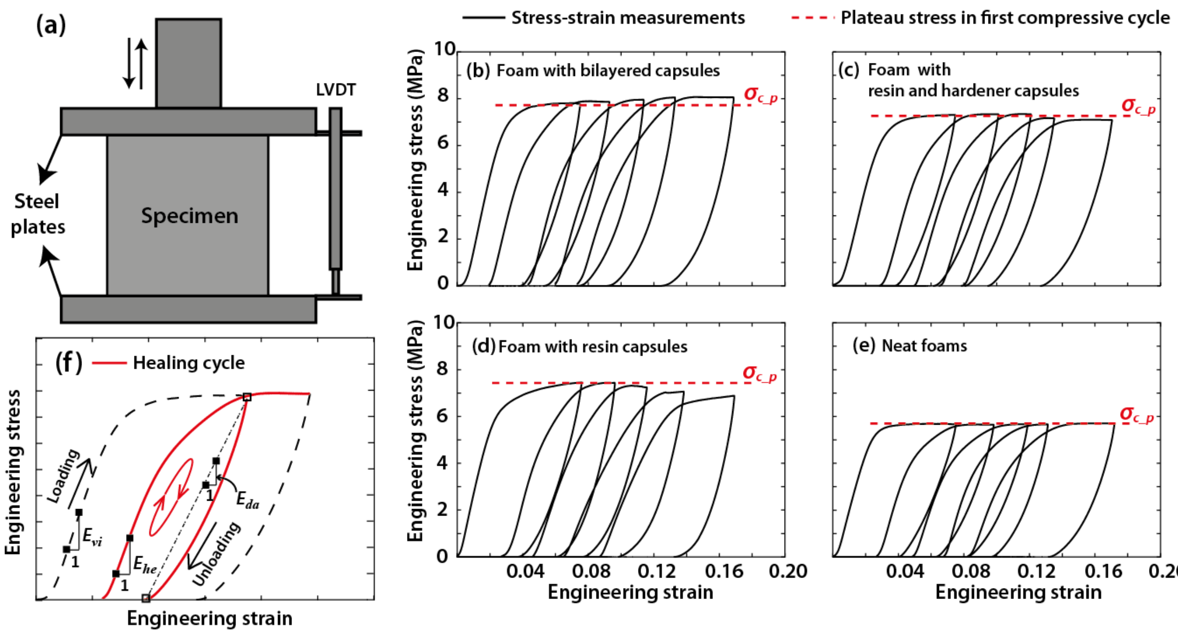

Figure 4. (a) The schematic of the cyclic quasi-static compression test. (b) – (e): The representative responses of a foam embedded with the bilayered capsules (b), a foam embedded with the resin and hardener capsules (c), a foam embedded with the resin capsules (d), and a neat foam (e) under cyclic quasi-static compression. Elastic moduli of loading and unloading are defined based on the loading-unloading stress-strain curve (f).

Quasi-static uniaxial compressive tests of capsules

To understand the compressive behaviours of the alginate capsules, the single-particle quasi-static compressive tests were carried out using an Instron testing machine at room temperature. Resin capsules, hardener capsules, and bilayered capsules were tested with four repetitions, respectively. The displacements were obtained by the average measurements recorded by two parallel LVDTs, as shown in Fig. 5 (a) schematically. The loading speed was 0.3 mm/min.

Fig. 5 shows the measured quasi-static compressive responses of three types of capsules. For hardener capsules, the compressive forces increase gradually during the compression, as shown in Fig. 5 (a). For resin and bilayered capsules, the measurements feature the similar yield forces, which are higher than those of hardener capsules in comparison of Fig. 5 (b) and (c) with (a). The compressive responses indicated that the resin layer dominated the compressive behaviour of the bilayered capsules.

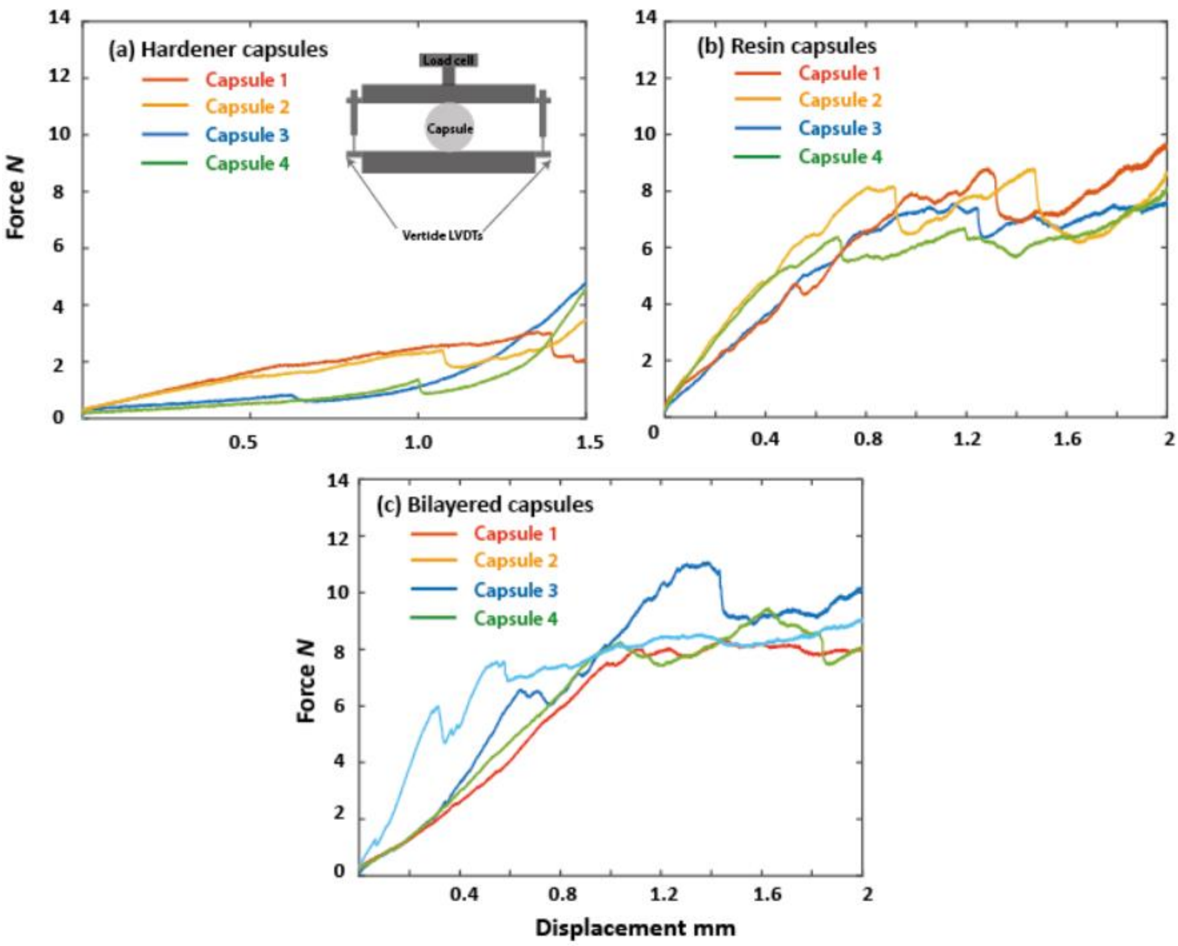

Figure 5. Compressive responses of (a) hardener capsules, (b) resin capsules, and (c) bilayered capsules.

3.2. Mechanical tests of the constitutive materials of the sandwich beams

In this study, the core shear cracks in the foam cores of sandwich beams were aimed to be healed. To trigger the core shear cracks, three-point bending tests were conducted, and the geometry of the sandwich beams was designed based on the mechanical properties of constituent materials. Quasi-static compressive and shear tests were conducted on the foams embedded with short glass fibres and capsules. Tensile and compressive tests were conducted on the glass fibre reinforced epoxy laminates. Three repetitions were tested for each type of specimen.

Quasi-static compressive and shear tests of fibre reinforced polymer foams

The compressive tests of the fibre reinforced foams with the dimension of 50mm X 50mm X 50mm followed the Standard ASTM 1621-04a. The compressive force P_F and the vertical displacement Δl of the crosshead were recorded by a 50KN load cell and an LVDT, respectively. The typical stress-strain curves of the fibre reinforced foam and the foam without fibre reinforcements are shown in Fig. 6 (a). The average compressive strength and elastic modulus of the fibre reinforced foam were 12.41 MPa and 430.12 MPa, respectively, which were both higher than those of the foam without fibre reinforcements. The shear tests of fibre reinforced foams with the dimension of 140mm X 40mm X 10mm followed the Standard ASTM C273. The specimens were bonded by two steel plates on the top and bottom faces using the Loctite EA 9461 two-part adhesive. The shear force was imposed by loading two parallel mild steel plates in opposite directions, as shown in Fig. 6 (b) schematically. A constant crosshead displacement rate of 0.5 $\mathrm{mm/min}$ was adopted. The average shear strength and shear modulus were 2.348 MPa and 209.144 MPa, respectively, measuring from the shear stress-strain curve.

Compressive and tensile tests of glass fibre reinforced composites

Compressive and tensile tests with $\pm 45^0$ loading orientation were conducted on the glass fibre reinforced epoxy laminates with six $\pm 45^0$ woven layers, and followed the Standard ASTM D3410M – 16 and Standard D 3039M, respectively. An Instron 2630 clip-on extensometer was used to measure the strain, which was confirmed by the Stingray F-146B Firewire Camera video gauge with Imentrum post-processing Video Gauge software. The nominal stress was measured from a 50KN load cell. Fig 6 (c) plots the compressive and tensile stress-strain curves of the laminates with the average strength of 505.32 MPa and elastic modulus of 33.91

GPa in tension, as well as the average strength of 413.68 MPa and elastic modulus of 23.83 GPa in compression.

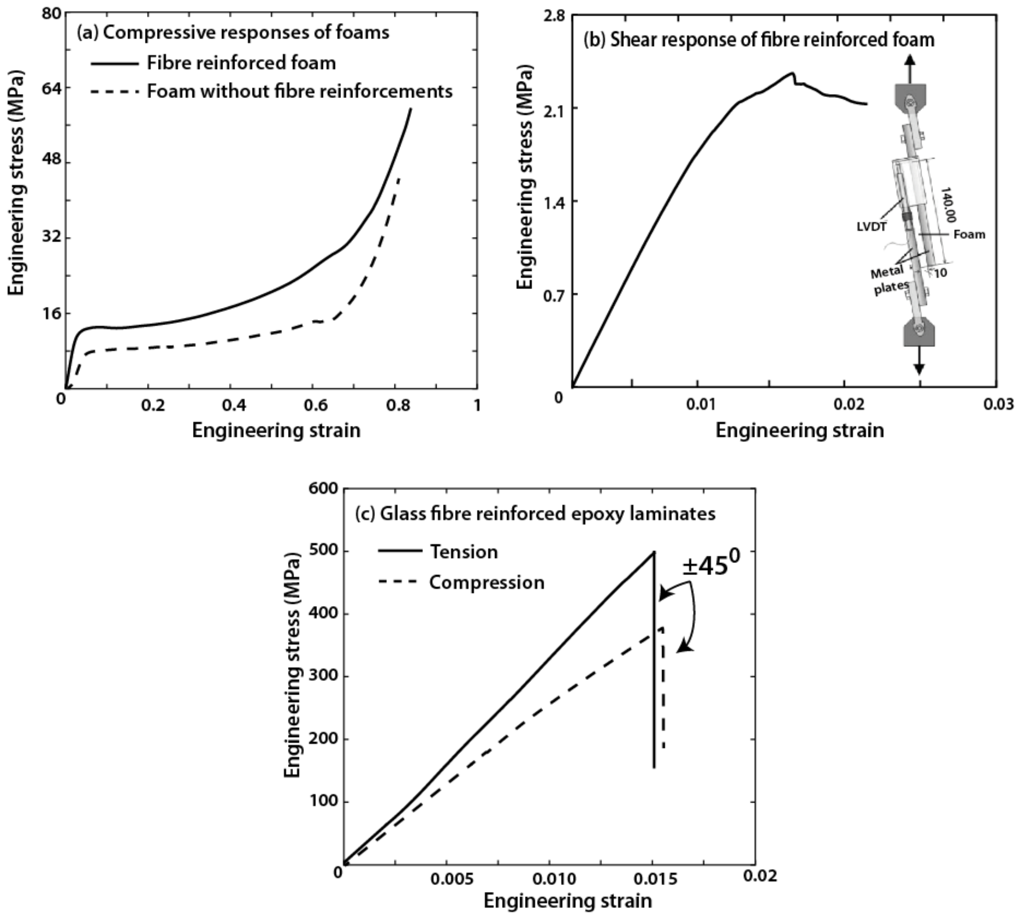

Figure 6. (a) Comparisons of the compressive responses between the fibre reinforced foam and the foam without fibre reinforcements. (b) The typical shear stress-strain curve for the fibre reinforced foam. (c) The typical stress-strain curves in tension and compression for the glass fibre reinforced epoxy laminates loading in $\pm 45^0$ loading orientation.

3.3. Geometry design of sandwich beams and three-point bending tests

A sandwich beam under simply supported three-point bending may fail with one of the following failure modes, i.e. face yielding, core shear, wrinkling of the face sheet, and indentation of the core material. The failure loads can be calculated as

$$P_{fy} = \frac{4\sigma_h b_h t_h d_h}{l_{s0}} \tag{1}$$

for face yielding,

$$P_{cs} = 2\tau_f b_h d_h \tag{2}$$

for core shear,

$$P_{wf} = \frac{2bt_h d_h}{l_{s0}} \sqrt[3]{E_h E_f G_f} \tag{3}$$

for wrinkling of face sheet, and

$$P_{ci} = b_h t_h \left(\frac{\pi^2 \sigma_f^2 E_h d_h}{3l_{s0}}\right)^{1/3} \tag{4}$$

for core indentation beneath the loading rollers. σ_f, τ_f, E_f, G_f represent the compressive strength, shear strength, elastic modulus, and shear modulus of foam core, respectively; σ_h, E_h represent strength and elastic modulus of face sheet, respectively; t_h, b_h, d_h, l_{s0} represent the thickness of face sheet, the width and thickness of sandwich beam, as well as the free span between two supports, respectively, as shown in Fig. 7. In this study, sandwich beams were designed based on the relation $P_{cs} < [P_{fy}, P_{fw}, P_{ci}]$ to trigger the failure mode of core shear under the three-point bending test. From the analytic equations and the mechanical properties of constitutive materials, the thickness of facesheets and length of sandwich beams were chosen as $t_h = 2.2$ mm and $l_h = 240$mm, respectively. The width and thickness of sandwich beam were $b_h = 40$mm and $d_h = 15$mm, respectively. The thickness of foam core is $t_f = 10$ mm. The geometry of the sandwich beam and the setup of the three-point bending test are schematically shown in Fig. 7, where l_0 is the free span between two supports. The three-point bending tests followed the Standard ASTM C393. The beams were loaded by a cylindrical roller with a radius of 10 mm, and the free span between two fixed supports was $l_{s0} = 170$mm.

The load was measured via a 20KN load cell, and the displacement before failure was measured via an LVDT. The LVDT was placed at centre of the bottom face. The displacement-controlled crosshead speed was 0.5 mm/min, and the loading was stopped after the peak force. To evaluate the self-healing effects, reloading was conducted after 24 hours from the previous loading to achieve stable results. The geometry of the sandwich beam and the setup of the three-point bending test are schematically shown in Fig. 7.

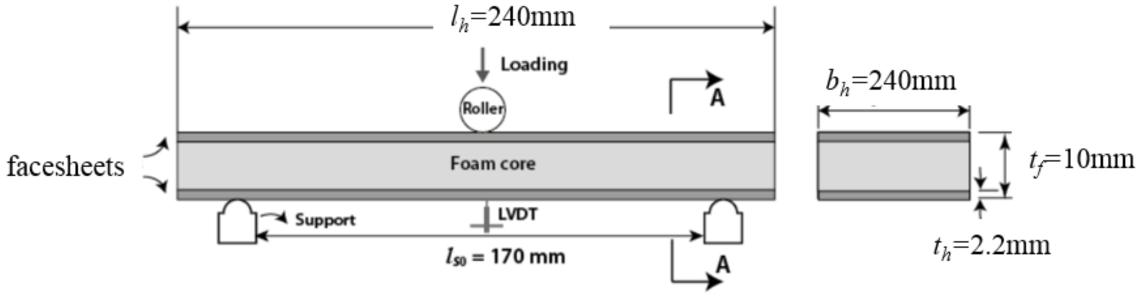

Figure 7. The geometry of the sandwich beam and the experimental setup of the three-point bending test.

3.4. Sandwich beams under high-speed soft impact tests

Sandwich structures used in the aerospace and marine applications may suffer from the impact damage. To examine the self-healing performance of foam cores sandwich structures after impact damage, high-speed soft impact tests were conducted [35] using the experimental setup shown in Fig. 8 (a). The geometry of the sandwich beams used in soft impact tests was identical to that used in three-point bending tests. Before the tests, the sandwich beams were fixed into a steel fixture, which was bolted into an aluminium alloy frame by eight M6 bolts. The distance from the gas gun muzzle to the front face of the specimens was 200mm. The length of the gas gun barrel was 3.5m with the outer diameter 40mm and the inner diameter 28mm. The Alporas® aluminium foam of density $\rho_p = 0.34\,\mathrm{g/cm^3}$, Young's modulus $E_{pf} = 1.0\ \mathrm{GPa}$ and plateau stress $\sigma_{pf} = 2.2\ \mathrm{MPa}$ were used to manufacture cylindrical projectiles, which had the length of $l_p = 40\mathrm{mm}$ and the diameter of $d_p = 27.5\mathrm{mm}$. The projectiles were accelerated through the gas gun barrel by compressed air that stored in a gas cylinder. Calibration tests were performed to ensure the projectiles hitting at the centre of the beams. Two laser gates were installed at the open end of the barrel to record the velocities of the accelerated projectiles. The exiting velocities of projectiles v_p were 246-290 $\mathrm{m/s}$, which corresponded to the momentum per unit area $I_p = \rho_p l_p v_p$ between 3.38 kPa•s and 3.70 kPa•s. A Phantom Mercury HS v 12.1 high-speed camera captured the images of projectiles impacting on the centre of the front face sheets and the back-face deflection of the beams. Typically, the recordings were set as the 22,000 fps frame rate, and 35 μs exposure time. To examine the self-healing effect after the high-speed soft impact tests, the damaged sandwich beams were tested under three-point bending tests 24 hours post the impact test.

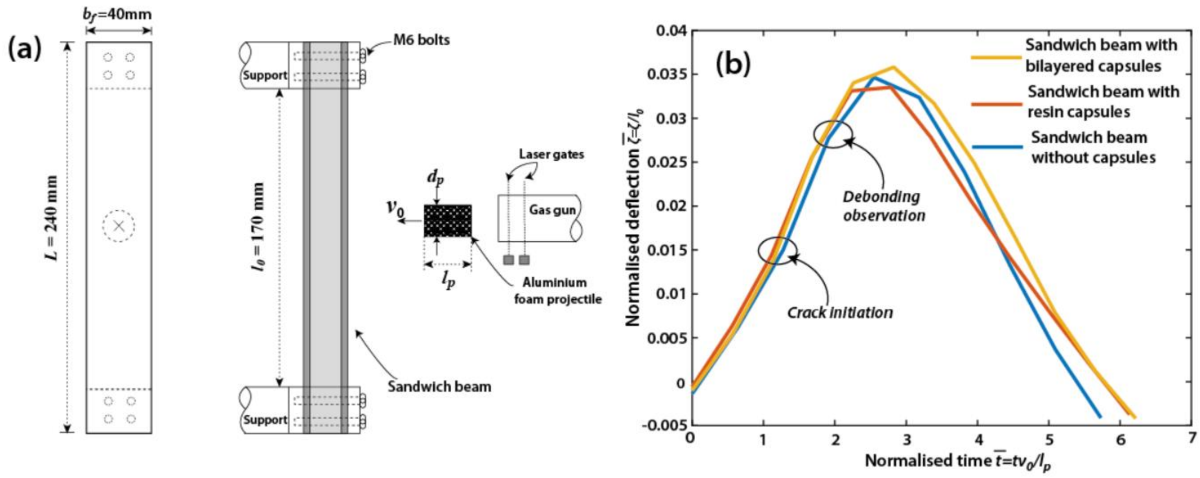

Figure 8. (a) The experimental setup of the high-speed soft impact test. (b) Comparison of normalised deflection $\bar{\zeta}$ as a function of normalised time $\bar{t}$ among three types of sandwich beams.

Figure 9 presents the montages of three types of sandwich beams under metal foam soft impact, obtained from the Phantom Mercury HS v 12.1 high-speed camera , i.e. sandwich beams with bilayered capsules (projectile velocity $290\ \mathrm{m/s}$ or momentum per unit area $I_p = 3.70\ \mathrm{kPa{\bullet}s}$) ; sandwich beams with resin capsules (no healing , projectile velocity $246\ \mathrm{m/s}$ or $I_p = 3.38\ \mathrm{kPa{\bullet}s}$) ; and sandwich beam without capsules (no healing , projectile velocity $290\ \mathrm{m/s}$ or $I_p = 3.70\ \mathrm{kPa{\bullet}s}$) . The shear cracks in the foam cores occured between $t = 170 \sim 250\ \mu\mathrm{s}$. The de-bonding between foam cores and face sheets was captured at approximately $t = 255\ \mu\mathrm{s}$.

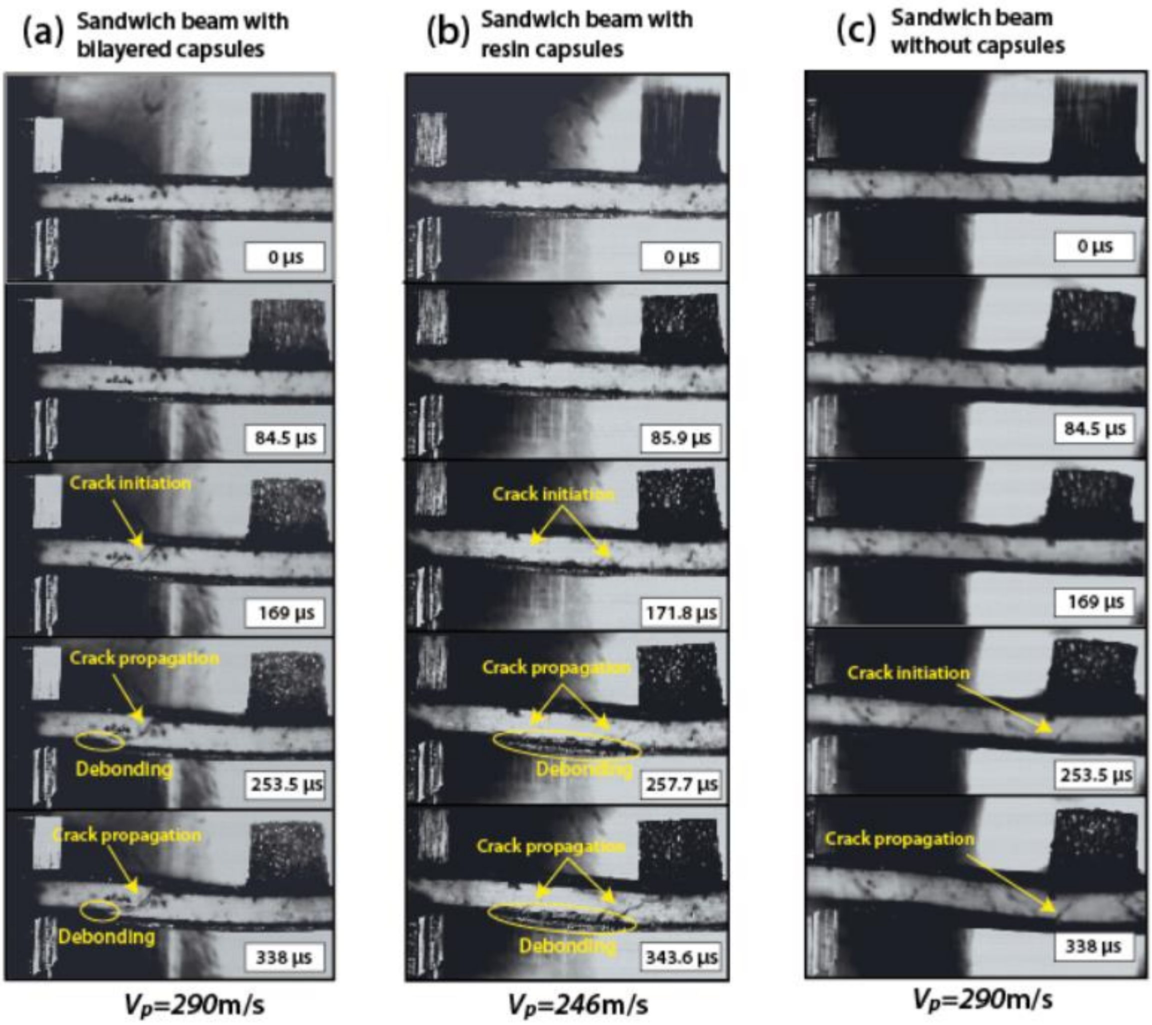

Figure 9. Montages obtained from the high-speed camera show the responses of (a) sandwich beam with bilayered capsules, (b) sandwich beam with resin capsules, and (c) sandwich beam without capsules under soft impact.

4. Results and discussion

4.1. Self-healing under cyclic quasi-static compression tests

As embedding capsules could result in modification of the mechanical properties of the matrix materials [37, 38], we first questioned whether the embedded capsules could enhance the strength and modulus of the polymer foams. The typical compressive responses of the foams embedded with bilayered capsules, foams embedded with dual capsules, foams embedded with resin capsules, and neat foams are shown in Fig. 4 (b), (c), (d), and (e), respectively. The compressive strength σ_c and elastic modulus E_c of the foams embedded with capsules in the 1st compression cycle are 7.35 MPa and 316.73 MPa, respectively, which are higher than those of neat foams (5.63 MPa for strength and 272.57 MPa for elastic modulus). This confirms that capsules have reinforcing effect to the matrix foams. The plateau stress σ_{c_p} of four types of foams in the 1st compression cycle is shown as the dashed line in Figs. 4. The plateau stress of the foam embedded with bilayered capsules increases gradually with the increments of compression cycles, while the plateau stress of the foam embedded with the dual capsule system and that of the neat foam remain the same. In contrast, the plateau stress of the foam embedded with resin capsules gives a decreased trend with the increments of the compression cycles. The results indicate that (1) foams embedded with capsules may have higher level damage owing to the localisation induced by capsules embedded in the foam matrix; and (2) the bilayered capsule system and the dual capsule system can maintain the plateau stress through the healing effect. The current healing mechanism is designed to heal the micro-cracks, however, the yielding of the foam is mainly controlled by the cells buckling under compression [39]. Hence, the healing effect on the plateau stress is limited.

In this research, a healing cycle is defined as the period from the unloading phase in the previous compression cycle to the loading phase in the current compression cycle, highlighted by the solid curve in Fig. 4 (f). To evaluate the healing effect in each healing cycle, the healing efficiency η is calculated as the recovered elastic modulus to the damaged elastic modulus $\eta = (E_{he} - E_{da})/(E_{vi} - E_{da})$ [40], where E_{vi} is the virgin elastic modulus in the first loading; E_{da} is elastic modulus after damage in the unloading phase; E_{he} is the healed elastic modulus obtained in the loading phase, indicating the healing effects. The elastic modulus of E_{vi}, E_{he} and E_{da} are determined based on the stress-strain curves in Fig. 4 (f) [41]. The relations between η and the healing cycles for four types of foams are shown in Fig. 10. For the neat foams and foams embedded with resin capsules (without healing), the values of healing efficiency η were non-zero, which were caused by the difference between the elastic moduli in the loading and unloading phases in one healing cycle. The absorption of air during unloading could be the reason to cause the difference [42]. Therefore, the healing effects can be evaluated based on the threshold value $\eta_s = 0.234$ that is equivalent to the healing efficiency calculated for the neat foam at the first healing cycle, i.e. there is healing effect if $\eta > \eta_s$, otherwise, no healing effect. The threshold η_s is highlighted by the horizontal dashed lines in Fig. 10 (a). The values of the healing efficiency η calculated for the foams embedded with resin capsules (without healing effects) are smaller than those of neat foams at the corresponding healing cycles, which indicates that embedding capsules into foams could result in more damage. For the foams embedded with bilayered capsules and dual capsules, the values of η in the 1st and 2nd healing cycles are higher than η_s, as shown in Fig. 10 (c) and (d), respectively, which indicates the presence of the multiple healing effects. The healing effects diminish in the 3rd healing cycle as the values of η are lower than η_s. For the alginate capsules with multicore-like or irregular honeycomb-like internal microstructures, as reported in this and previous researches [43], multiple healing events could be achieved owing to release of the residual healing agents stored in the undamaged pores inside damaged capsules. With increment of healing cycles, the amount of the stored healing agents decrease, which cause the decrease of healing efficiency. In comparison, the capsules with core-shell structure can only show single healing event due to the complete release of healing agents after breaking of capsules [23, 42]. The values of η for the foams embedded with bilayered capsules are higher than those of foams embedded with dual capsules in each corresponding healing cycle. This indicates that the bilayered capsules system can provide better healing efficiency than the conventional dual capsules system: the uneven distribution of dual capsules could cause the insufficient chemical reaction of the two-part healing agents, which limits the healing efficiency [18].

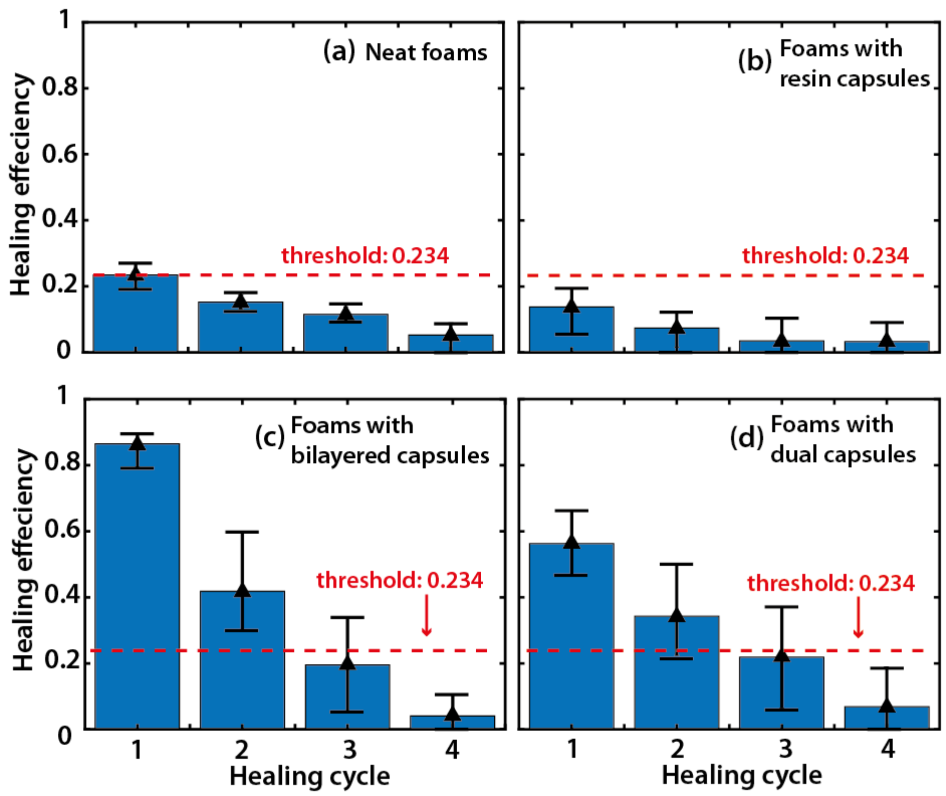

Figure 10. The relations of the healing efficiency against the healing cycle of (a) neat foams, (b) foams embedded with resin capsules, (c) foams embedded with bilayered capsules, and (d) foams embedded with dual capsules under cyclic compressive tests.

The optical microscope and SEM were used to investigate the healing effect of the foams embedded with bilayered capsules. Figure 11 (a) shows that the released healing agents could provide good covering on the damaged surface. After the polymerisation of the healing agents, the interconnected cracks were completely healed by the polymerised film. The interface between the polymerised film and the foam surface is shown in Fig. 11 (b). Figure 11 (c) shows the surface of a foam containing a healed crack, a partially healed crack, and an unhealed crack. The partially healed crack is further investigated using SEM, as shown in Fig. 11 (d) for example. Either insufficient released healing agents or the premature completion of healing agent polymerisation could cause the incompletely healing.

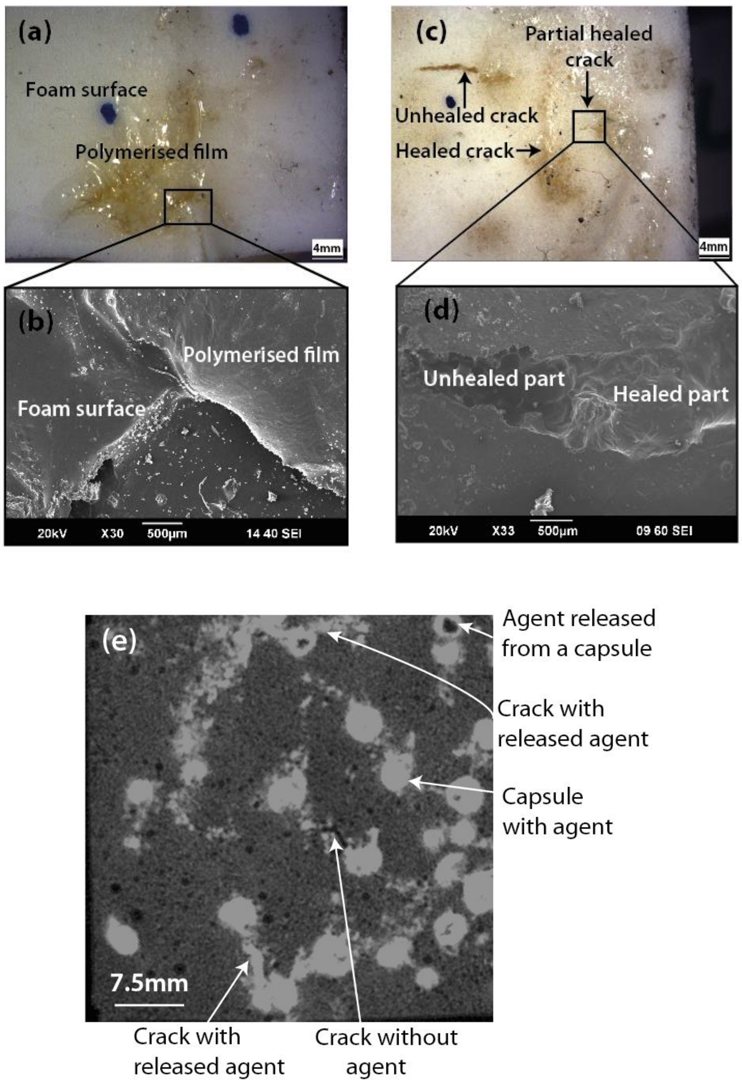

Figure 11. (a) An optical microscopy image showing the good cover of the polymerised film on the interconnected cracks; (b) a SEM image showing the selected region in (a); (c) an optical microscopy image showing healed and unhealed cracks; (d) a SEM image of the selected region in (d); (e) an X-ray microcomputed tomography image showing a cross-section of a foam sample embedded with bilayered capsules after damage.

X-ray microcomputed tomography (μCT) was employed to reveal the healing mechanism of the foams embedded with bilayered capsules, as shown in Fig. 11 (e). The pixels of the X-ray image were chosen as 714x714 to obtain the image with good quality. After the 1st compression cycle, capsules, healed micro-cracks and unhealed micro-cracks were visible as the white particles, white lines, and black lines, respectively. The white lines linking the two adjacent capsules indicated the flowing of the released healing agents through the micro-cracks. As the bilayered capsules could retain healing agents after the 1st compression cycle, shown as the white particles in Fig. 11 (e), the bilayered capsules system could achieve multi-healing effect.

To evaluate the effect of volume fraction (VF) of the bilayered capsules to the self-healing performance, cyclic quasi-static compressive tests were conducted on the foams embedded with 5% and 15% VF bilayered capsules. The typical compressive responses of three types of foams are shown in Fig. 12 (a) to (c), respectively. The results indicated that the elastic modulus and strength of the foam increased with the increase of the VF of the capsules. The healing efficiency η of three types of foams are plotted in Fig. 12 (d). The threshold value $\eta_s = 0.234$ was selected to evaluate the healing effects. In the 1st healing cycle, all three types of foams showed healing effects. The values of η of foams embedded with 10% and 15% VF capsules were similar and higher than those of foams embedded with 5% VF of capsules. With the increments of healing cycles, polymer foams embedded with higher VF bilayered capsules provided better η as more healing agents could be released.

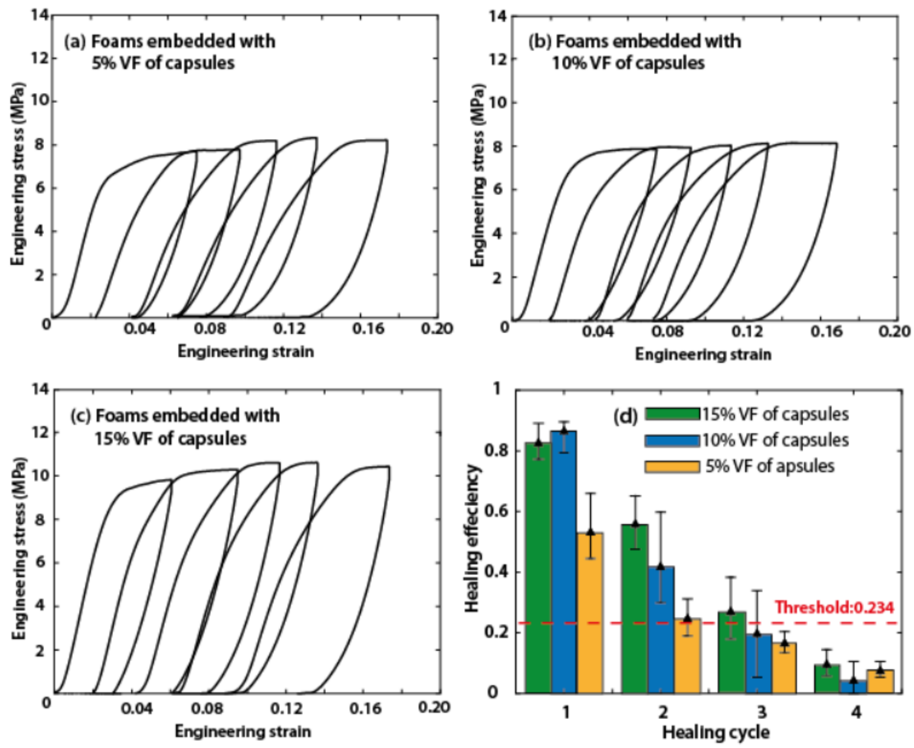

Figure 12. (a) – (c): The typical compressive responses of (a) foams embedded with 5% VF of bilayered capsules, (b) foams embedded with 10% VF of bilayered capsules, and (c) foams embedded with 15% VF of bilayered capsules. (d) The comparisons of the healing efficiency among the foams embedded with 5%, 10%, and 15% VF of bilayered capsules.

4.2. Self-healing of foam core sandwich beams under three-point bending

As higher VF of capsules could offer better healing effects, the foam cores with 15% VF of bilayered capsules were used to manufacture sandwich beam samples, see Section 2.10. The foam core sandwich beams containing 15% VF of resin capsules and neat foam core sandwich beams, both without healing effects, were tested as the control groups. The overall damage of the sandwich beams under three-point bending may be ascribed to (1) shear damage within the foam cores; (2) damage in facesheets; and (3) interfacial damage between facesheets and cores. The proposed healing system can contribute to recovery of the damage of foam cores and the interfacial damage, and may have negligible effect to recover the damage in facesheets. The normalised elastic modulus $\tilde{E}_t$ was used to evaluate the healing effect as it can give direct comparison between the samples with healing and without healing, which can be calculated as

$$\tilde{E}_t = E_r / E_v \tag{5}$$

where E_v is the virgin flexural modulus measured in the 1st loading, and E_r the flexural modulus measured at the reloading stage. Both E_v and E_r can be calculated as $E_{t\,\mathrm{or}\,v} = \triangle P_t l_0^3 / 4\triangle\zeta_t b_t d_t^3$, where $\triangle P_t$ is the increment of load, and $\triangle\zeta_t$ the increment of displacement. $\triangle P_t / \triangle\zeta_t$ represents the slope of the linear portion of the load–displacement curve, which takes the contributions of both foam cores and face sheets into account. Figures 13 (a) – (c) show the typical load-displacement curves of the three types of sandwich beams under three-point bending tests, respectively. The beam samples subjected to 3 loading-unloading cycles. Only the load-displacement curves measured at loading phases are shown in the figures. In the 1st loading, the average flexural moduli for three types of sandwich beams are similar, which indicate that embedding capsules do not have a noticeable effect on flexural modulus. In the 1st or 2nd reloading, the sandwich beams with bilayered capsules exhibit higher flexural modulus than those of the control groups owing to recovery of damage by the healing system. The tests stopped after the 2nd reloading when the significant debonding between foam cores and face sheets occurred. The relations between the normalised flexural modulus and the number of reloading are shown in Fig. 13 (d). To evaluate the healing effect, we use a threshold value $\tilde{E}_{ts} = 0.421$, which is equivalent to the value of $\tilde{E}_t$ of the neat foam core sandwich beam at the 1st reloading. The healing effect is evident if the measured value of $\tilde{E}_t$ is higher than the threshold value $\tilde{E}_{ts}$, which is highlighted by the horizontal dashed lines in Fig. 13 (d). For the sandwich beams embedded with resin capsules (without healing), the values of $\tilde{E}_t$ were lower than those of the neat foam core sandwich beams, which again indicated that embedding capsules into foams could result in more damage. For the sandwich beams containing bilayered capsules, the value of $\tilde{E}_t$ in the 1st reloading could be recovered to up to 0.8 after healing. Owing to the debonding between foam cores and facesheets, the healing effect diminished during the 2nd reloading cycle (the value of $\tilde{E}_t$ drops below $\tilde{E}_{ts}$). However, the sandwich beams with bilayered capsules still exhibited higher flexural modulus compared to the sandwich beams without healing system as the damage had been partially recovered by the healing system.

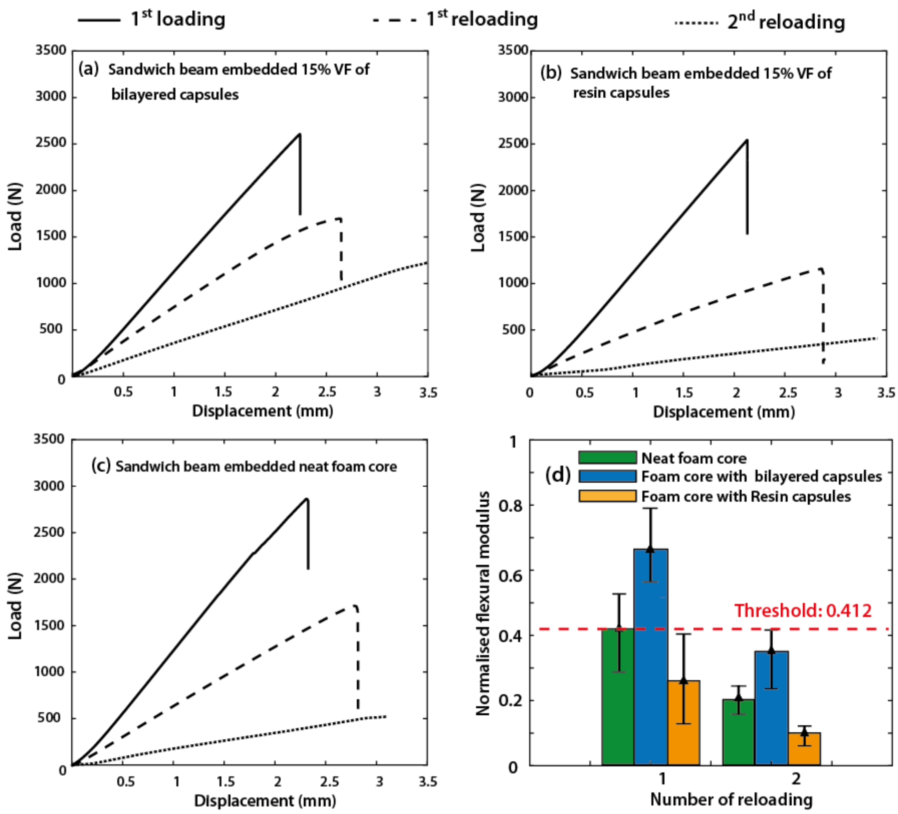

Figure 13. The typical load-displacement measurements of (a) the sandwich beam with foam core embedded with bilayered capsules, (b) the sandwich beam embedded with resin capsules, and (c) the sandwich beam with neat foam cores under three-point bending tests. (d) The normalised flexural modulus $\tilde{E}_t$ against the number of reloading for the three types of sandwich beams.

Figure 14 (a) shows a sandwich beam with bilayered capsules under three-point bending tests, which demonstrated that the failure mode was core shear. After the test, the damaged region was cut and analysed by SEM. The SEM images suggested that cracks could be healed by the released healing agents, as shown in Fig. 14 (b) for example. This could cause partial recovery of the flexural modulus. For the comparison purpose, the failure mode of a sandwich beam with resin capsules (without healing effects) is shown in Fig. 14 (c), and the SEM image of an unhealed core shear crack is shown in Fig. 14 (d). Without healing, the core shear crack could propagate to the interface between the bottom facesheet and the foam core to cause significant debonding.

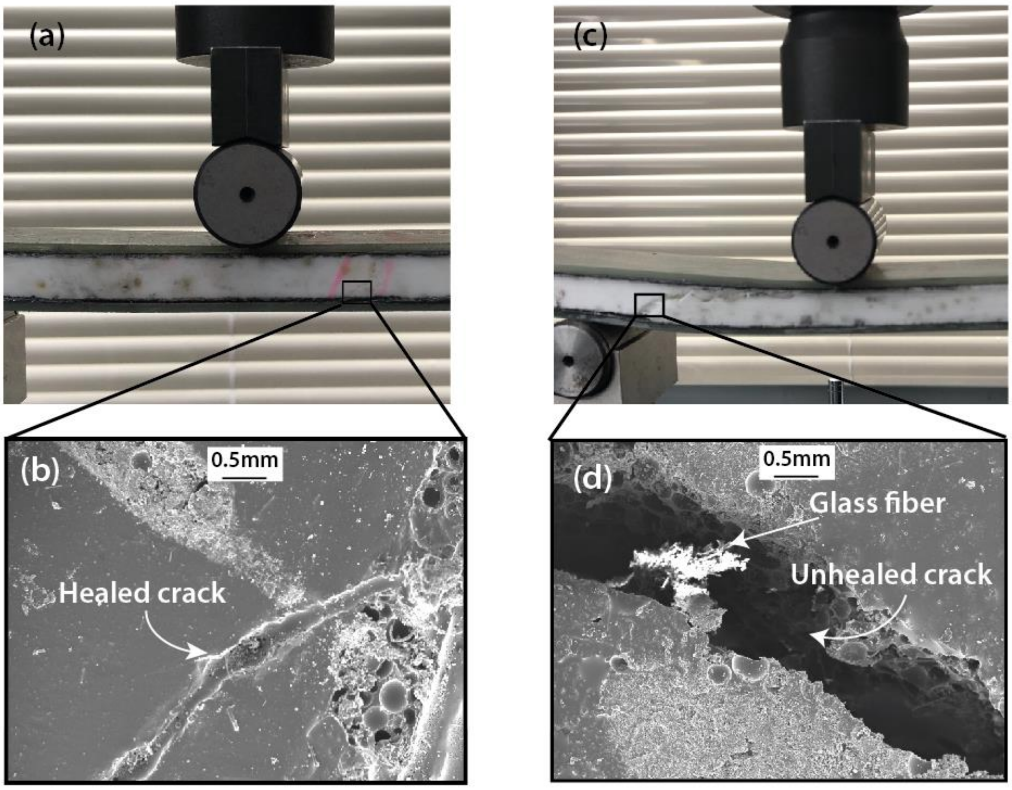

Figure 14. (a) and (c) The photographs of sandwich beams with bilayered capsules and with resin capsules under three-point bending tests, respectively. (b) and (d) The SEM images of a healed crack and an unhealed crack from the selected regions in (a) and (c), respectively.

4.3. Self-healing of foam core sandwich beams under high-speed soft impact

The geometry of fibre-reinforced sandwich beams used in the high-speed soft impact tests were the same as those used in the three-point bending tests. To characterise the impact responses of the sandwich beams, the functional relations between normalised time $\bar{t} = tv_0/l_p$ and normalised deflection $\bar{\zeta} = \zeta/l_o$ were measured for the sandwich beams with bilayered capsules, sandwich beams with resin capsules and sandwich beams without capsules, respectively, as shown in Fig. 8 (b) , where t denotes the time measured after contact between the aluminium projectile and the sandwich beams; v_0 and l_p the velocity and length of the projectiles, respectively ; ζ the back-face deflection of the beam at the centre span; and l_o the free span between two fixtures. The responses of three types of sandwich beams during the impact were similar, which indicated that embedding capsules did not have a noticeable effect on the impact responses of the sandwich beams. The peak back face deflection occurred at around $\bar{t} = 3$, which suggested that the transient deformations of sandwich beams had completed after the densification $(\bar{t} = 1)$ of the projectiles [35]. Under high speed soft impact, core shear cracking occurred followed by debonding between cores and back facesheets, see Fig. 15 (a). The self-healing system can contribute to recovery of the damage within foam cores. To evaluate the healing effect, three-point bending test was conducted on the damaged sandwich beams 24 hours post the impact tests. The measured responses from the three-point bending test of the three types of sandwich beams before and after soft impact are shown in Fig. 15 (b), (c) and (d), respectively. To evaluate the healing effect, normalised residual elastic flexural modulus $\tilde{E}_t = E_r / E_v$ was calculated based on the measurements, where E_r is the flexural modulus of the damaged beams measured post soft impact, E_v the virgin flexural modulus measured before soft impact, as summarised in Fig. 15 (e). Comparing the responses of sandwich beams with resin capsules and sandwich beams without capsules, both without self-healing effect, embedding capsules into a foam could again result in higher level damage during the soft impact as sandwich beams without capsules exhibited higher residual elastic modulus. With the presence of self-healing system, i.e. the bilayered capsules system, the sandwich beams could achieve higher residual elastic flexural modulus compared to sandwich beams without capsules. To examine the healing mechanism, SEM was employed to examine the healing of cracks within the foam cores before the three-point bending testing, as shown in Fig. 15 (a) for example, which suggested that the shear cracks could be partially healed by the released healing agents post impact. However, the healing effect was limited as the self-healing system had negligible healing effect on the damage within the facesheets and debonding.

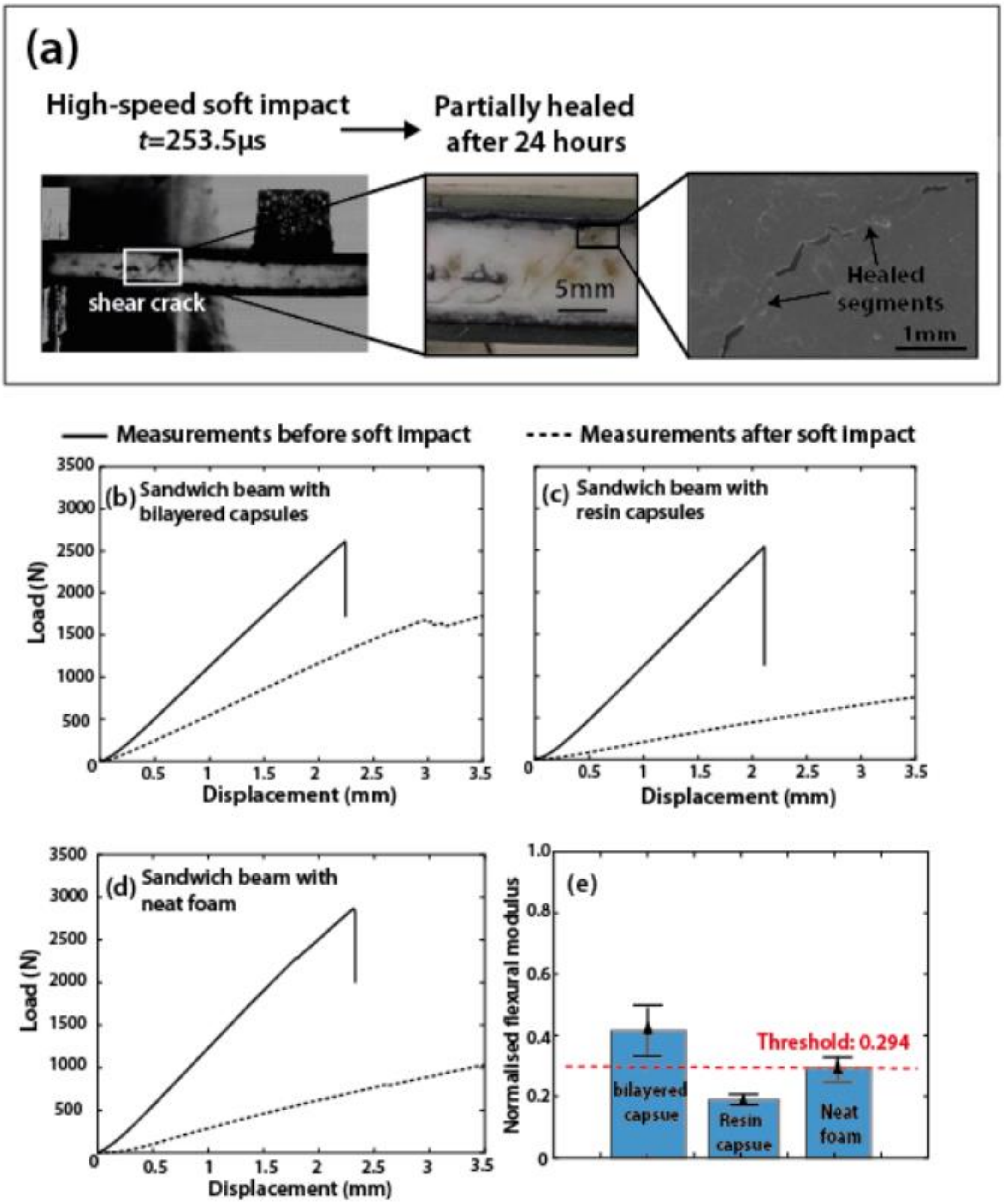

Figure 15 (a) a sandwich beam embedded with bilayered capsules under the high-speed soft impact test. The partially healed micro-crack was observed via SEM post the impact tests. The representative responses of the sandwich beam with a foam core embedded with bilayered capsules (b), the sandwich beam with a foam core embedded with resin capsules (c), and the sandwich beam with a neat foam core (d) before and post impact tests. (e) The comparisons of the normalised residual elastic flexural modulus $\tilde{E}_t$ of the three types of sandwich beams.

5. Concluding remarks

In this research, we reported a novel, multi-stage encapsulation process that can encapsulate two mutually reactive healing agents (epoxy resin and hardener) within single multicore-like bilayered calcium-alginate capsules. Quasi-static cyclic compression tests were conducted to evaluate the mechanical behaviours and self-healing performances of the polymer foams embedded with bilayered capsules. It was demonstrated that the presence of the bilayered capsules in the foams could enhance the compressive strength and stiffness, and the bilayered capsules showed better multiple self-healing performances compared to the conventional dual capsule system. Three-point bending and high-speed soft impact tests were conducted to evaluate the self-healing effects to foam cored sandwich beams. The experimental study suggested that the bilayered capsules did not have a noticeable reinforcing effect on the flexural modulus without damage, however it could provide a noticeable self–healing effect when the damage occurred.

As a pioneering study on the bilayered capsules based self-healing system, there are still several issues that need to be addressed in the future study. The diameter of bilayered capsules will need to be further decreased to the micron level, which could expand the applications to epoxy coatings and fibre-reinforced polymer composites. After the drying process in capsules fabrication, the residual water could still remain within capsules, which may affect the healing effects. The effect of the residual water will be under further investigation. Further mechanical tests will be conducted to evaluate the self-healing performances of bilayered capsule systems under different loading conditions, such as fracture and fatigue.

Acknowledgments

The authors acknowledge the support from the Defence of Science and Technology Laboratory, UK (DSTL, DSTLX-1000104239). The first author would like to acknowledge the financial support of the China Scholarship Council (CSC, 201606240017).

References

[1] M.L. Jr., K. Branner, H.N. Petersen, J. Beauson, M. Mcguan, B.F. Sørensen, Materials for Wind Turbine Blades: An Overview, Materials 10 (2017) 1285. https://doi:10.3390/ma10111285.

[2] D. Li, S. C. M. Ho, G. Song, L. Ren, H. Li, A review of damage detection methods for wind turbine blades. Smart Mater. Struct. 24 (2015), 33001. https://doi.org/10.1088/0964-1726/24/3/033001.

[3] M.L. Jr, H.W. Zhou, H.Y. Yi, L.L. Gui, R.D. Peng, H.W. Wang, Microscale damage mechanisms and degradation of fibre-reinforced composites for wind energy applications: results of Danish–Chinese collaborative investigations, J. Compos. Mater. 48 (2014) 2977-2991. https://doi:10.1177/0021998313503876.

[4] M. McGuan, G. Pereira, B.F. Sørensen, H. Toftegaard, K. Branner, Damage tolerance and structural monitoring for wind turbine blades, Philos. Trans. R. Soc. A 373 (2015) 20140077. https://doi.org/10.1098/rsta.2014.007.

[5] R. Herring, K. Dyer, F. Martin, C. Ward, Renew, The increasing importance of leading edge erosion and a review of existing protection solutions, Sustain. Energy Rev. 115 (2019), 109382. https://doi.org/10.1016/j.rser.2019.109382.

[6] M. Szekalska, A. Pucilowska, E. Szymanska, P. Ciosek, K. Wiinicka, Alginate: Current Use and Future Perspectives in Pharmaceutical and Biomedical Applications, Int. J. Polym. Sci. 2016 (2016), 1-17. https://doi.org/10.1155/2016/7697031.

[7] B.J. Blaiszik, S.L.B. Kramer, S.C. Olugebefola, J.S. Moore, N.R. Sottos, S.R. White, Self-healing polymers and composites, Annu. Rev. Mater. Res. 40 (2010) 179-211. https://doi.org/10.1146/annurev-matsci-070909-104532.

[8] S.D. Bergman, F. Wudl, Mendable polymers, J. Mater. Chem. 18 (2008) 41-62. https://doi.org/10.1039/b713953p.

[9] J. Nji, G. Li, Damage healing ability of a shape-memory-polymer-based particulate composite with small thermoplastic contents. Smart Mater. Struct. 21 (2012) 25011. https://doi.org/10.1088/0964-1726/21/2/025011.

[10] S. A. Hayes, W. Zhang, M. Branthwaite, F. R. Jones, Self-healing of damage in fibre-reinforced polymer-matrix composites, J. R. Soc. Interface 4 (2007) 381-387. https://doi.org/10.1098/rsif.2006.0209.

[11] S. A. Hayes, F. R. Jones, K. Marshiya, W. Zhang, A self-healing thermosetting composite material, Compos. Part A-Appl. S. 38 (2007) 1116-1120. https://doi.org/10.1016/j.compositesa.2006.06.008.

[12] G. Li, M. John, A self-healing smart syntactic foam under multiple impacts, Compos. Sci. Technol. 68 (2008) 3337-3343. https://doi.org/10.1016/j.compscitech.2008.09.009.

[13] M. John, G. Li, Self-healing of sandwich structures with a grid stiffened shape memory polymer syntactic foam core, Smart Mater. Struct. 19 (2010) 075013. https://doi.org/10.1088/0964-1726/19/7/075013.

[14] R.S. Trask, H.R. Williams, I.P. Bond, Self-healing polymer composites: mimicking nature to enhance performance, Bioinspir. Biomim. 2 (2007) 1-9. https://doi.org/10.1088/1748-3182/2/1/p01.

[15] C.J. Hansen, S.R. White, N.A. Sottos, J.A. Lewis, Accelerated Self-Healing Via Ternary Interpenetrating Microvascular Networks, Adv. Funct. Mater. 21 (2011) 4320-4326. https://doi.org/10.1002/adfm.201101553.

[16] T. Al-Mansoori, R. Micaelo, I. Artamendi, J. Norambuena-Contreras, A. Garcia, Capsules for self-healing of asphalt mixture without compromising mechanical performance, Constr. Build Mater. 115 (2017) 1091-1100. https://doi.org/10.1016/j.conbuildmat.2017.08.137.

[17] T. Sun, X. Shen, C. Peng, H. Fan, M. Liu, Z. Wu, A novel strategy for the synthesis of self-healing capsule and its application, Compos. Sci. Technol. 171 (2019), 13-20. https://doi.org/10.1016/j.compscitech.2018.12.006.

[18] Y. Wang, D.T. Pham, C. Ji, E. Harkin-jones, Self-healing composites: A review, Cogent Eng. 2 (2015) 1075686. https://doi.org/10.1080/23311916.2015.1075686.

[19] H. Jin, C.L. Mangun, A.S. Griffin, J.S. Moore, N.R. Sottos, S.R. White, Thermally Stable Autonomic Healing in Epoxy using a Dual-Microcapsule System, Adv. Mater. 26 (2013), 282–287. https://doi.org/10.1002/adma.201303179.

[20] E.N. Brown, S.R., White, N.R. Sottos, Retardation and repair of fatigue cracks in a capsule toughened epoxy composite—Part II: In situ self-healing, Compos. Sci. Technol. 65 (2005) 2474-2480. https://doi.org/10.1016/j.compscitech.2005.04.053.

[21] M.M. Caruso, D.A. Delafuente, V. Ho, N.R. Sottos, J.S. Moore, S.R. White, Solvent-Promoted Self-Healing Epoxy Materials, Macromolecules 40 (2007) 8830-8832. https://doi.org/10.1021/ma701992z.

[22] I.L. Hia, V. Vahedi, P. Pasbakhsh, Self-Healing Polymer Composites: Prospects, Challenges, and Applications, Polym. Rev. 56 (2016) 225–261. https://doi.org/10.1080/15583724.2015.1106555

[23] Y.C. Yuan, M.Z. Rong, M.Q. Zhang, Jian. Chen, G.C. Yang, X.M. Li, Self-Healing Polymeric Materials Using Epoxy/Mercaptan as the Healant, Macromolecules 41 (2008) 5197-5202. https://doi.org/10.1021/ma800028d.

[24] L.L. Hia, E.S. Chan, S.P. Chai, P. Pasbakhsh, A novel repeated self-healing epoxy composite with alginate multicore capsules, J. Mater. Chem. A 6 (2018) 8470-8478. https://doi.org/10.1039/c8ta01783b.

[25] Q. Li, Siddaramaiah, N.H. Kim, D. Hui, J.H. Lee, Effects of dual component capsules of resin and curing agent on the self-healing efficiency of epoxy, Compos. Part B-Eng. 55 (2013) 79-85. https://doi.org/10.1016/j.compositesb.2013.06.006.

[26] S.R. White, N.R. Sottos, P.H. Geubelle, J.S. Moore, M.R. Kessler, S.R. Sriram, E.M, Brown, S. Viswanathan, Autonomic healing of polymer composites, Nature 409 (2001) 794. https://doi.org/10.1038/35057232.

[27] J.M. Kamphaus, J.D. Rule, J.S. Moore, N.R. Sottos, S.R. White, A new self-healing epoxy with tungsten (VI) chloride catalyst, J. Royal Soc. Interface 5 (2008) 95-103. https://doi.org/10.1098/rsif.2007.1071.

[28] X. Liu, X. Sheng, J.K. Lee, M.R. Kessler, J.S. Kim, Rheokinetic evaluation of self-healing agents polymerised by Grubbs catalyst embedded in various thermosetting systems, Compos. Sci. Technol. 69 (2009) 2102-2107. https://doi.org/10.1016/j.compscitech.2008.08.024.

[29] T.S. Coop, U.F.J. Mayer, D.F. Wass, R.S. Trask, I.P. Bond, Self-Healing of an Epoxy Resin Using Scandium(III) Triflate as a Catalytic Curing Agent, Adv. Funct. Mater. 21 (2011) 4624-4631. https://doi.org/10.1002/adfm.201101660.

[30] J. Wu, M.D. Weir, M.A.S. Melo, H.H.K. Xu, Development of novel self-healing and antibacterial dental composite containing calcium phosphate nanoparticles, J. Dent. 43 (2015) 317-326. https://doi.org/10.1016/j.jdent.2015.01.009.

[31] M.M. Caruso, B.J. Blaiszik, S.R White, N.R. Sottos, J.S. Moore, Full Recovery of Fracture Toughness Using a Nontoxic Solvent-Based Self-Healing System, Adv. Funct. Mater. 18 (2008), 1898-1904. https://doi.org/10.1002/adfm.200800300.

[32] L. Yuan, S. Huang, A. Gu, G. Liang, F. Chen, Y. Hu, S. Nutt, A cyanate ester/capsule system with low cure temperature and self-healing capacity, Compos. Sci. Technol. 87 (2013) 111-117. https://doi.org/10.1016/j.compscitech.2013.08.005.

[33] R. T. Quazi, S.N. Bhattacharya, E. Kosior, The effect of dispersed paint particles on the mechanical properties of rubber toughened polypropylene composites, J. Mater. Sci. 34 (1999) 607-614. https://doi.org/10.1023/A:1004515300637.

[34] O. E. Sotomayer, H. V. Tippur, Role of cell regularity and relative density on elastoplastic compression response of 3-D open-cell foam core sandwich structure generated using Voronoi diagrams, Acta Mater. 78 (2014) 301-313. https://doi.org/10.1016/j.actamat.2014.06.051.

[35] P. Turner, T. Liu, X. Zeng, Dynamic Response of Orthogonal Three-Dimensional Woven Carbon Composite Beams under Soft Impact, J. Appl. Mech. 82 (2015) 121008. https://doi.org/10.1115/1.4031455.

[36] B.P. Russell, T. Liu, N.A. Fleck, V.S. Deshpande, Quasi-Static Three-Point Bending of Carbon Fibre Sandwich Beams With Square Honeycomb Cores, J. Appl. Mech. 78 (2011) 031008. https://doi.org/10.1115/1.4003221.

[37] R. T. Quazi, S.N. Bhattacharya, E. Kosior, The effect of dispersed paint particles on the mechanical properties of rubber toughened polypropylene composites, J. Mater. Sci. 34 (1999) 607-614. https://doi.org/10.1023/A:1004515300637.

[38] S. Cao, T. Liu, A. Jones, W. Tizani, Particle reinforced thermoplastic foams under quasi-static compression, Mech. Mater. 136 (2019) 103081. https://doi.org/10.1016/j.mechmat.2019.103081.

[39] L.J. Gibson, M.F. Ashby, Cellular Solids, second ed., Cambridge University Press. 1997. https://doi.org/10.1017/CBO9781139878326

[40] E.J. Barbero, K.J. Ford, Characterization of Self-Healing Fibre-Reinforced Polymer-Matrix Composite with Distributed Damage, J. Adv. Mater. 39 (2007) 20-27.

[41] Z. Lu, P. Blackmore, J.L. Rover, Cyclic Stress-Strain Behaviour of AM60B and AE44 Cast Magnesium Alloys and Its Impact on LCF Characterisation and Fatigue Analysis, SAE Int. J. Mater. Manf. 7 (2014) 446-453. https://doi.org/10.4271/2014-01-0969.

[42] M. Petrů, O. Novák, Measurements and Numerical Modelling of Mechanical Properties of Polyurethane Foams, in: Aspects of Polyurethane, IntechOpen, Rijieka, Croatia, 2017, pp. 73-109. https://doi.org/10.5772/intechopen.69700.

[43] L.L. Hia, P. Pasbakhsh, E.S. Chan, S.P. Chai, Electrosprayed Multi-Core Alginate Microcapsules as Novel Self-Healing Containers, Sci. Rep. 6 (2016) 34674. https://doi.org/10.1038/srep34674.